Journal of Nuclear Materials 404 (2010) 154–159

Contents lists available at ScienceDirect

Journal of Nuclear Materials

journal homepage: www.elsevier.com/locate/jnucmat

Creep properties of annealed Zr–Nb–O and stress-relieved Zr–Nb–Sn–Fe cladding tubes and their performance comparison

S. Ko [a], S.I. Hong [a,*], K.T. Kim [b]

[a] Department of Nano-Materials Engineering, Chungnam National University, Yusung, Daejon 305-764, Republic of Korea
[b] College of Energy and Environment, Dongguk University (Kyungju Campus), Kyungsangbukdo 780-714, Republic of Korea

ARTICLE INFO

Article history:
Received 5 April 2010
Accepted 12 July 2010

ABSTRACT

Creep properties of annealed Zr–Nb–O and stress-relieved Zr–Nb–Sn–Fe cladding tubes were studied and compared. The creep rates of the annealed Zr–Nb–O alloy were found to be greater than those of the stress-relieved Zr–Nb–Sn–Fe alloy. Zr–Nb–O alloy was found to have stress exponents of 5–7 independent of stress level whereas Zr–Nb–Sn–Fe alloy exhibited the transition of the stress exponent from 6.5 to 7.5 in the lower stress region to ~4.2 in the higher stress region. The reduction of stress exponent at high stresses in Zr–Nb–Sn–Fe can be explained in terms of the dynamic solute–dislocation effect caused by Sn atoms. The constancy of stress exponent without the transition was observed in Zr–Nb–O alloy, supporting that the decrease of the stress exponent with increasing stress in Zr–Nb–Sn–Fe is associated with Sn atoms. The difference of creep life between annealed Zr–Nb–O and stress-relieved Zr–Nb–Sn–Fe is not large considering the large difference of strength level between annealed Zr–Nb–O and annealed stress-relieved Zr–Nb–Sn–Fe. The better-than-expected creep life of annealed Zr–Nb–O alloy can be attributable to the combined effects of creep ductility enhancement associated with softening and the decreased contribution of grain boundary diffusion due to the increased grain size.

1. Introduction

The Zr alloy cladding tube has served as one of the key structural materials in nuclear power reactors since it has shown high temperature strength, corrosion resistance, good mechanical properties, and low neutron absorption [1]. The cladding's in-reactor behaviors such as corrosion, mechanical strength, creep and irradiation-induced growth may be mainly controlled by its alloying elements and heat treatment conditions applied in the pilgering processing [2–4]. Based on in-reactor experience of various Zr alloys, it is generally found that Sn increases mechanical strength and creep resistance but decrease corrosion resistance [4,5], while Nb increases corrosion and irradiation-induced growth resistance [4,6]. It was also found that the higher heat treatment temperature after the final pilgering step lowered the mechanical strength but enhanced the corrosion and growth resistance [5]. Therefore, stress relieved claddings may be favored if relatively higher mechanical strength is required, while fully recrystallized cladding is favored if better corrosion and growth resistance are needed [4,5].

It is noteworthy that, in Zirlo™ (trademark of Westinghouse Electric Co.), Nb was added to increase the corrosion resistance, but Sn was reduced to increase the corrosion resistance with the moderate mechanical strength. The Zirlo™ tube was heat-treated in the stress relieved condition after cold pilgering to render the better mechanical strength and creep strength. In M5™ (trademark of AREVA NP), Nb was also introduced, but Sn was eliminated for the better corrosion resistance at the expense of the mechanical strength. The M5™ tube was heat-treated in the recrystallized condition to render the better corrosion resistance and growth resistance also at the expense of the mechanical strength. The concern about the lower mechanical strength of M5 may be mitigated by the fact that the mechanical strength will be drastically increased even with slight irradiation in-reactor [7–9]. However, controversy remains over the trade-off between the enhanced corrosion resistance and the lower strength in M5™ that could weaken the creep resistance is beneficial or at least allowable for the reliability of cladding tubes and nuclear fuels. In this study, creep deformation behaviors of recrystallized Zr–Nb–O and stress-relieved Zr–Nb–Sn–Fe cladding tubes were examined and their creep performance comparison was made along with the microstructural analyses. The understanding of the difference of creep behaviors between annealed Zr–Nb–O and stress-relieved Zr–Nb–Sn–Fe cladding tubes in this study may be utilized for the optimization of thermo-mechanical processing aimed at the enhanced creep performance of cladding tubes.

* Corresponding author. Tel.: +82 42 821 6595; fax: +82 42 822 5850.
E-mail address: sihong@cnu.ac.kr (S.I. Hong).

0022-3115/$ - see front matter © 2010 Elsevier B.V. All rights reserved.
doi:10.1016/j.jnucmat.2010.07.023

Table 1
Chemical composition of Zr alloys (w/o).

Element	Nb	Sn	Fe	Cr	O	Zr
Zr–Nb–Sn–Fe	1.0	1.0	0.1	–	0.11	Bal.
Zr–Nb–O	1.0	–	–	–	0.15	Bal.

2. Experimental methods

In this study, annealed Zr–Nb–O and stress-relieved Zr–Nb–Sn–Fe alloy cladding tubes were selected for studies of mechanical behaviors and creep characteristics. Both alloys were manufactured by cold pilgering with intermediate heat treatments. Zr–Nb–O cladding tubes were heat-treated at 560 °C for 5 h and Zr–Nb–Sn–Fe alloy cladding tubes were stress-relieved at 460 °C for 7 h after final cold pilgering. Chemical compositions of the two Zr alloys are given in Table 1. In order to examine the microstructural stability of cladding tubes at high temperatures, the same Zr alloy tubes were additionally heat-treated at 500 °C and 600 °C for 8 h and examined by optical microscopy.

In order to examine the creep characteristics in the circumferential direction, the Zr alloy rings with the width of 4 mm were cut vertically against the axial direction of tubes. In this study, a special grip with two half-cylinders with 1 mm wide space between them was used to strain the ring specimen with maintaining a circular configuration of the ring in contact with the grips all the way during the tests [10,11]. The radius of the half-cylinders was 4.35 mm, which is a half of the inner diameter of the cladding tubes. It was experimentally confirmed that the deformation occurred in the left and right-hand sides of the ring within 5 mm width centered on the split line of two half-cylinders and the optimum gage length was assumed to be 5 mm [10–12]. The load was applied to the ring specimen against the surface of the half cylinder and the force normal to the surface of half cylinder due to the applied load is close to zero in left and right-hand sides of the ring. The force normal to the surface of half cylinder increases rapidly away from these both sides and becomes maximum on the bottom and top parts of the ring, resulting in the drastic increase of the friction force and negligible deformation outside the gage length centered on the split line of two half-cylinders.

Constant stress creep testers were used to investigate the creep deformation mechanisms of Zr alloys. The tensile testing was performed at room temperature, 450, 480 and 500 °C, while the creep tests were performed at 450, 480 and 500 °C with the applied stress between 80 and 150 MPa. For microstructural analyses, transmission electron microscopy (TEM) specimens were made from the crept rings in the steady-state creep region. TEM specimens were examined by a TEM (JEOL-2010) equipped with an energy dispersive X-ray spectroscopy (EDS) detector with an accelerated voltage of 200 kV.

3. Results and discussion

Fig. 1 displays three-dimensional views of the Zr–Nb–Sn–Fe (a–c) and Zr–Nb–O (d–f) alloy cladding tubes, with a post-pilgering heat treatment (a, d) and heat-treated additionally for 8 h at 500 °C (b, e) and 600 °C (c, f), respectively. As seen in this figure, very fine elongated grains in the pilgering direction were observed after a post-pilgering heat treatment (annealing in Zr–Nb–O and stress relieving in Zr–Nb–Sn–Fe), whereas equi-axed grains were observed after the additional heat treatments at 500 °C and 600 °C for 8 h and the grain size increased with increase of heat treatment temperature. More cold-work energy was thought to be stored along the tube axis during cold pilgering and the driving force for recrystallization along the tube axis is greater, resulting in more rapid and drastic recrystallization along the axial direction.

Table 2 shows average grain sizes of Zr alloys additionally heat-treated at 500 °C and 600 °C for 8 h after a post-pilgering heat treatment. It is noted that grain sizes prior to the additional heat treatment was difficult to measure using an optical microscope due to very fine grain sizes below 1 μm. After the additional heat treatment at 600 °C, the Zr–Nb–Sn–Fe alloy (3.5 μm) exhibited much finer grains than the Zr–Nb–O alloy (5.4 μm), as seen in Fig. 1 and Table 2. The grain size of Zr–Nb–Sn–Fe (3.2 μm) after heat treatment at 500 °C was also found to be finer than that of Zr–Nb–O (3.6 μm). It is known that Sn atoms in the Zr alloys may suppress grain boundary movement, retarding grain growth and making grains finer [13]. In general, the cold-worked metals are thermodynamically in an unstable state and internal energy accumulated during cold-working process is used as the driving force for recrystallization and grain growth [14]. The smaller grain size in Zr–Nb–Sn–Fe alloy tubes in comparison with that of Zr–Nb–O alloy tubes as seen in Fig. 1 and Table 2 can be explained by the

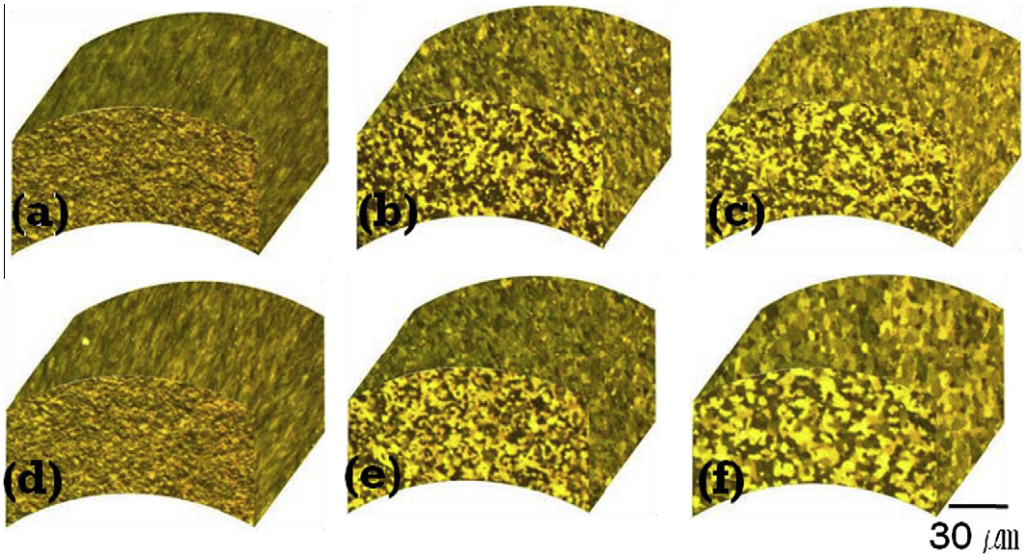

Fig. 1. Three-dimensional views of the Zr–Nb–Sn–Fe (a–c) and Zr–Nb–O (d–f) alloy cladding tubes, with a post-pilgering heat treatment (a, d) and heat-treated additionally for 8 h at 500 °C (b, e) and 600 °C (c, f).

Table 2
Grain size of Zr–Nb–Sn–Fe and Zr–Nb–O after post-pilgering heat treatment.

Alloy (°C)	Zr–Nb–Sn–Fe (μm)	Zr–Nb–O (μm)
500	3.2	3.6
600	3.5	5.4

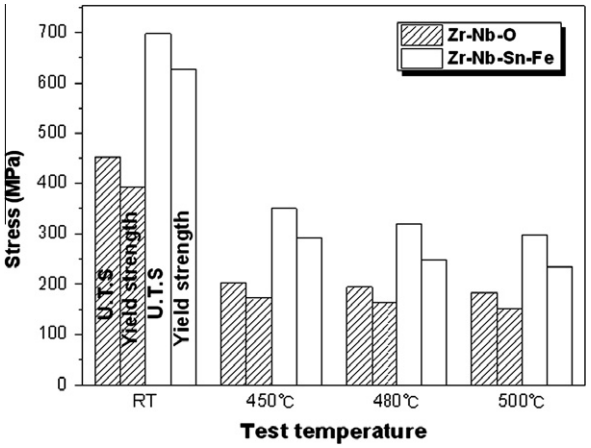

Fig. 2. Yield strengths and ultimate tensile strengths of annealed Zr–Nb–O and stress-relieved Zr–Nb–Sn–Fe at room temperature, 450, 480 and 500 °C.

difference of thermo-mechanical processing and a higher Sn content in Zr–Nb–Sn–Fe alloy.

The ultimate tensile and yield strengths of annealed Zr–Nb–O alloy and stress-relieved Zr–Nb–Sn–Fe alloy tubes at various temperatures are exhibited in Fig. 2. The strengths of Zr–Nb–Sn–Fe alloy tubes appear to have typical mechanical characteristics of stress-relieved Zr alloys and the strength decreased rapidly with the increase of temperature. The stress-relieved Zr–Nb–Sn–Fe alloy was observed to have the ultimate tensile and yield strengths ~40% greater than those of the annealed Zr–Nb–O alloy. The higher strength of Zr–Nb–Sn–Fe compared to Zr–Nb–O is attributed mostly to the combined effects of solid solution strengthening of Sn and the lower heat treatment temperature. The rapid decrease of mechanical strength up to 450 °C is likely to be caused by the release of internal cold-work energy resulting from dynamic recovery/recrystallization and the thermally-activated deformation with the increase of temperature.

Both annealed Zr–Nb–O and stress-relieved Zr–Nb–Sn–Fe displayed typical creep deformation curves consisting of the primary, secondary and tertiary periods as in Fig. 3. The circumferential creep strain was defined as the time dependent strain, $\varepsilon_t - \varepsilon_o$, the total strain ($\varepsilon_t$) subtracted by the initial instantaneous strain (ε_o) upon loading. As expected, the creep rates of annealed Zr–Nb–O alloy tubes were observed to be higher than those of stress-relieved Zr–Nb–Sn–Fe alloy tubes. On the other hand, the creep ductility in Zr–Nb–O alloy was found to be greater than in Zr–Nb–Sn–Fe. It should be noted in Fig. 3 that the total creep strain until fracture in Zr–Nb–O was in the range of 0.45–0.55 whereas that for Zr–Nb–Sn–Fe was in the range of 0.35–0.42. In Fig. 4, the steady-state creep rates of the two Zr alloys at 450, 480 and 500 °C are plotted against the stress. As expected, the steady-state creep rates of the Zr–Nb–O alloy tubes are relatively higher than those of the Zr–Nb–Sn–Fe alloy. However, the difference of steady-state creep rates between Zr–Nb–O alloy and Zr–Nb–Sn–Fe alloy is not as pronounced as that of tensile strength, which may explain the no reported significant creep-related integrity problems for Zr–Nb–O alloy tubes. The less pronounced difference of creep rates between annealed Zr–Nb–O and stress-relieved Zr–Nb–Sn–Fe could be associated

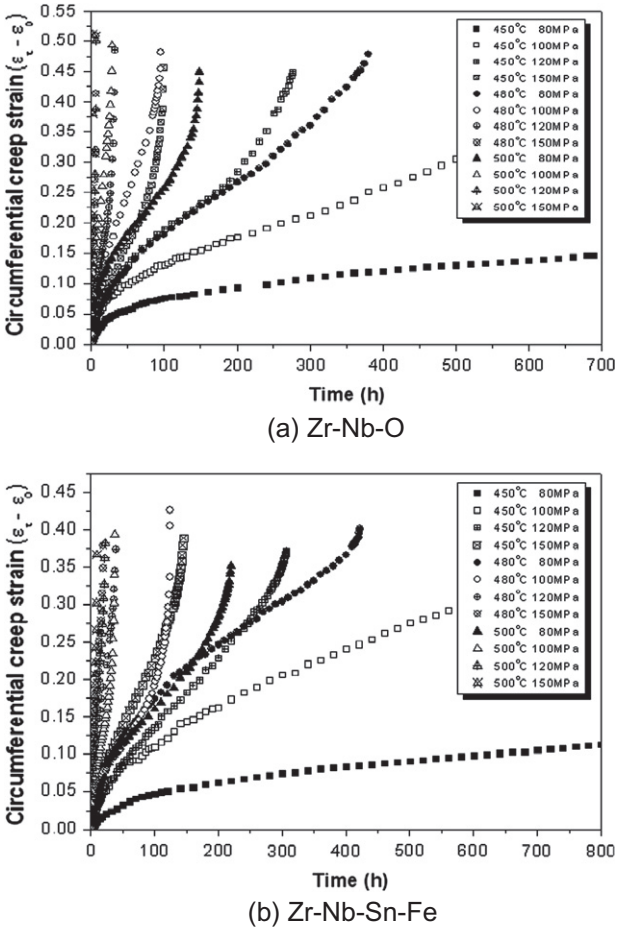

Fig. 3. Creep curves of Zr alloys: (a) annealed Zr–Nb–O, and (b) stress-relieved Zr–Nb–Sn–Fe.

with the less contribution of grain boundary diffusion due to a larger grain size in Zr–Nb–O which may have compensated for the lower strength.

In general, creep deformation at intermediate temperatures occurs as a result of thermally-activated motion of dislocations. Creep strain rate is usually expressed by the following power-law type relationship [15–17]:

$$\varepsilon = BD\sigma^n = A\sigma^n \exp(-Q_c/RT) \quad (1)$$

where ε is the steady-state creep rate, σ is the applied stress, A and B are material property-related constants, n is the stress exponent, Q_c is the activation energy for creep deformation, R is the gas constant and T is the absolute temperature. One interesting observation is that the stress exponent n remains constant (5–7) in the stress range of the present study for Zr–Nb–O whereas it decreases from 6.5 to 7.5 in the lower stress region to ~4.2 in the higher stress region for Zr–Nb–Sn–Fe.

The transition of the stress exponent from 5–7 to 3–4 have been associated with the transition of the creep deformation mechanism from the climb controlled creep to glide controlled creep [18,19]. Hong [20–23] explained the transition of the stress exponent in terms of the dynamic solute–dislocation interaction. In the dynamic solute–dislocation interaction model, the transition of the stress exponent from 5–7 to 3–4 can be attributed to the increasing solute drag stress due to dynamic solute–dislocation interaction with increase of creep rate (i.e. applied stress). The authors of the present study previously [11] suggested that the transition of the stress exponent from 5–7 to 3–4 in Zr–Nb–Sn–Fe

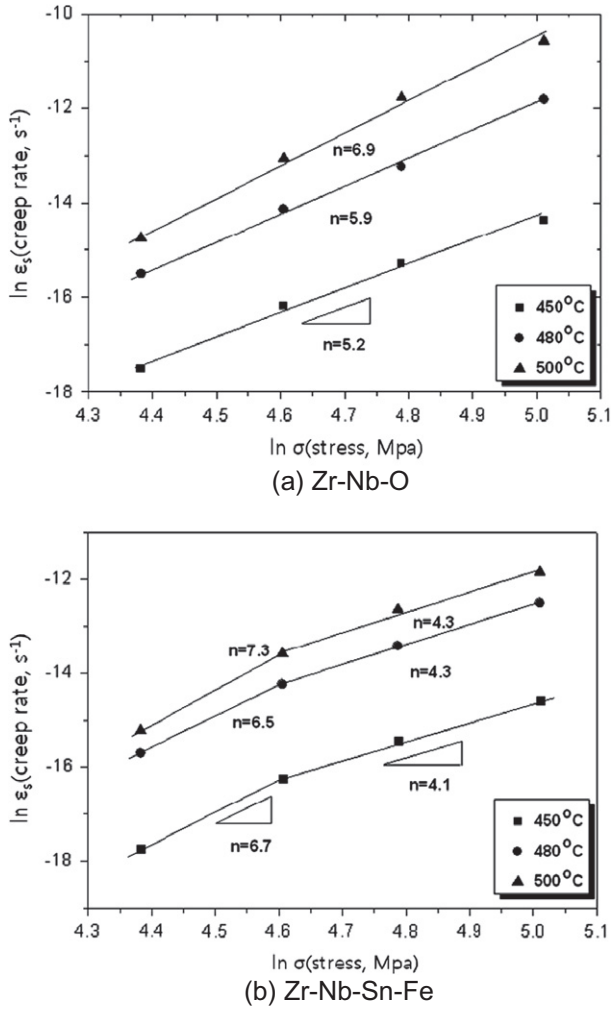

Fig. 4. Relationships between steady-state creep rate and stress for Zr alloys at 450, 480 and 500 °C: (a) annealed Zr–Nb–O, and (b) stress-relieved Zr–Nb–Sn–Fe.

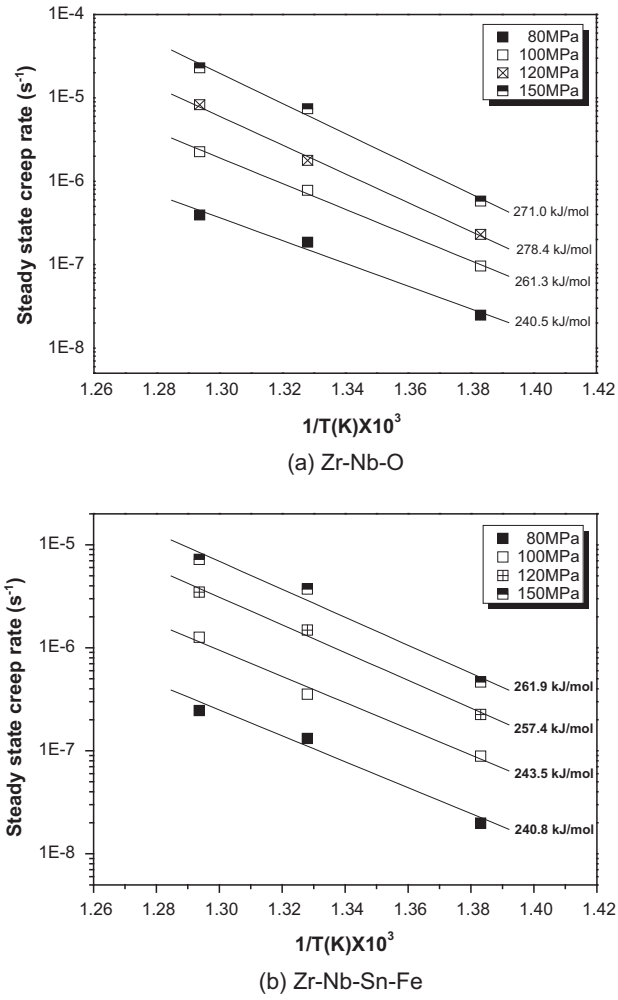

Fig. 5. Steady-state creep rate plotted against $1/T$ for Zr alloys at 450, 480 and 500 °C: (a) annealed Zr–Nb–O, and (b) stress-relieved Zr–Nb–Sn–Fe.

alloy and Zr–Sn–Fe–Cr alloy can be attributed to the increasing solute drag stress due to dynamic solute–dislocation interaction with increase of creep rate (i.e., applied stress) and that, in the temperature and strain rate range for creep of their study, Sn atoms are responsible for the transition of stress exponent [11]. The constancy of stress exponent without the transition was observed in Zr–Nb–O alloy tubes, strongly supporting that the decrease of the stress exponent with increasing stress in Zr–Nb–Sn–Fe is associated with the presence of Sn atoms. Lee et al. [11] suggested that Sn not only influences the gliding of dislocations and diffusion of vacancies [24] but also reduces the stacking fault energy of the Zr matrix [25]. Dislocation climb and/or cross slip becomes more difficult with the addition of Sn atoms because of a wider spacing between partial dislocations due to low stacking fault energy [26], resulting in the lower creep rates. It can be said that Sn is one of the key alloying elements reducing creep rate in Zr–Nb–Sn–Fe alloy. In Zr–Nb–O, the solute atoms which can be mobile and cause dynamic solute–dislocation interaction is oxygen atoms, but the temperature range in which oxygen atoms exert the maximum drag stress under creep condition is much lower than the creep temperature range of this study because oxygen atom is much smaller than Sn atom [26–28].

The activation energy of creep deformation can be derived by Eq (1) represented by the Arrhenius equation [15,16]. From Eq. (1), activation energy, Q_c can be written as $-R[(\partial \ln \varepsilon/\partial(1/T)]_\sigma$. Using this relationship, activation energies were calculated in Fig. 5. As seen in this figure, activation energy for creep in Zr–Nb–O was found to be slightly greater that in Zr–Nb–Sn–Fe. The activation energy for creep deformation is in the range of between 240 and 260 kJ/mol for the Zr–Nb–Sn–Fe alloy, while it is in the range of between 240 and 280 kJ/mol for the Zr–Nb–O alloy. The creep activation energy observed in this study is close to those of creep for Zircaloy-2 (245–287 kJ/mol [29]) and Zr (234–271 kJ/mol [30]). The slightly greater creep activation energy in Zr–Nb–O is thought to be attributed to the lower contribution of grain boundary diffusion due to a lager grain size. The increasing contribution of grain boundary diffusion is known to lower the activation energy for creep [31]. The rate controlling mechanism for Zr–Nb–O alloy is thought to be the dislocation climb controlled creep in which the stress exponent is typically in the range of 5–7 independent of the stress level.

Fig. 6 shows the TEM micrographs for the steady-state creep specimens of Zr–Nb–Sn–Fe (a) and Zr–Nb–O (b) tested at 480 °C at the applied stress of 80 MPa. As seen in Fig. 6b, dislocation networks and pile-ups around the precipitates are found in the Zr–Nb–O matrix. Dislocations were observed to be distributed more or less randomly in Zr–Nb–Sn–Fe (Fig. 6a) possibly due to the drag stress caused by Sn atoms. There appears to be little difference in the precipitate sizes (30–130 nm) between the Zr–Nb–Sn–Fe and Zr–Nb–O alloys. The precipitates in the Zr–Nb–O matrix are reported to be β-Nb phase with BCC structure and the precipitates

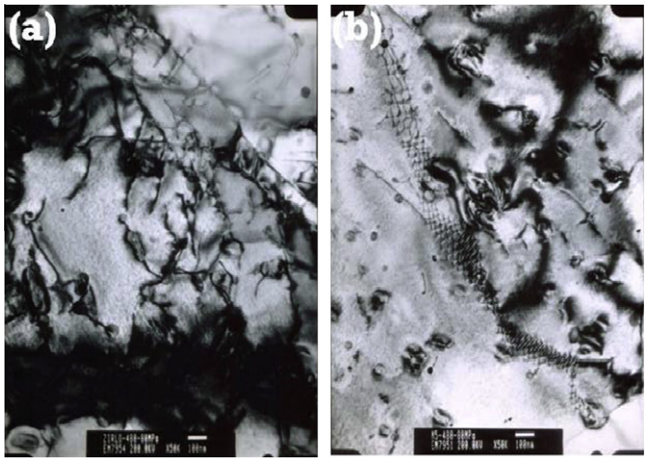

Fig. 6. TEM micrographs of Zr alloys at 480 °C: (a) Zr–Nb–Sn–Fe, and (b) Zr–Nb–O.

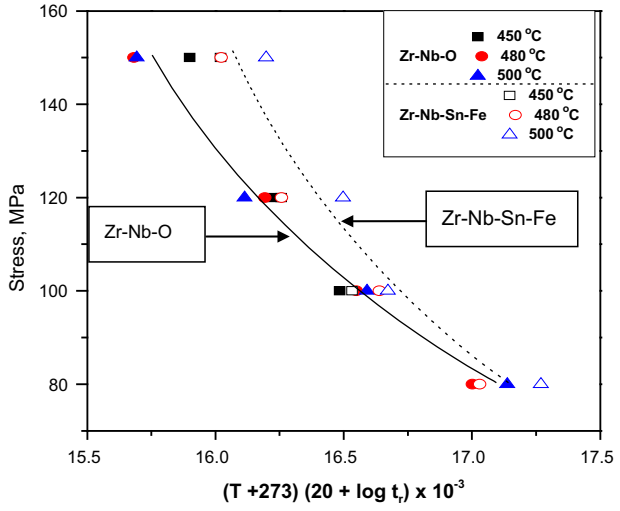

Fig. 7. Larson–Miller plot for Zr–Nb–O and Zr–Nb–Sn–Fe.

containing Fe alloying element as well as β-Nb precipitates were observed in Zr–Nb–Sn–Fe [32,33].

The integrity evaluation and life prediction of Zr alloy claddings are needed to maintain the safety of nuclear power plants and to improve its economical efficiency. Creep life decreases sharply with the increase of temperature and stress. Based on the relationship between stress, temperature and creep life, one can predict the creep life at various temperatures and stresses. In this study, Larson–Miller Parameter (LMP) was used to evaluate the creep life as follows [34]:

$$\mathrm{LMP} = TC + \log(t_r) \tag{2}$$

where T is temperature, C is the material-related constant and t_r is the creep life. The constant C is generally assumed to have a commonly used value of 20. Fig. 7 shows the relationship between applied stress and LMP. It can be seen that LMP decreases with the increase of applied stress. Mayuzumi and Onchi [35] found the creep rupture properties of stress-relieved Zircaloy-4 can be well expressed by the Lason–Miller Parameter.

One interesting observation is that the difference of LMP between annealed Zr–Nb–O and stress-relieved Zr–Nb–Sn–Fe is not large considering the large difference of strength level between annealed Zr–Nb–O and stress-relieved Zr–Nb–Sn–Fe (see Fig. 2). The difference of LMP between these two alloys decreased as the stress decreased. The better-than-expected creep life of annealed Zr–Nb–O alloy with a lower strength can be attributable to the of creep ductility enhancement associated with softening because the increased creep ductility mitigates the effect of the increased creep rate. Since the creep life can be approximated to be $\varepsilon_f/\dot{\varepsilon}_s$ (where ε_f is the creep strain until fracture and $\dot{\varepsilon}_s$ is the steady-state creep rate), the creep life would not decrease much if the fracture creep strain increases with the increase of steady-state creep rate. It appears that steady-state creep rate in the annealed Zr–Nb–O of the present study was not increased as much as the creep ductility as shown in Fig. 3 possibly because of the decreased contribution of grain boundary diffusion due to the decreased grain boundary fraction caused by the increased grain size.

The cladding tubes with a lower creep rate such as the stress-relived Zr–Nb–Sn–Fe may be favored if the dimensional stability is required under load controlled conditions whereas the annealed Zr–Nb–O could be favored if the higher failure strain is needed under strain controlled conditions. The optimum heat treatment condition after pilgering is thought to be dependent on the reactor operation conditions and remains to be explored in more depth. The creep behaviors of these alloys are expected to be substantially modified under irradiation and caution should be exercised in the application of the results obtained in this study.

4. Conclusions

Creep tests were performed for Zr–Nb–O and Zr–Nb–Sn–Fe and the results can be summarized as follows:

(1) The stress-relieved Zr–Nb–Sn–Fe alloy has ultimate tensile and yield strengths ~40% greater than those of the annealed Zr–Nb–O alloy. The higher strength of stress-relieved Zr–Nb–Sn–Fe may be attributed to the higher stored cold-work energy and solution strengthening due to Sn atoms.

(2) The out-of-reactor steady-state creep rates of the annealed Zr–Nb–O alloy was found to be greater than those of the stress-relieved Zr–Nb–Sn–Fe alloy in the temperature and stress range of this study, in compatible with the higher strengths of the stress-relieved Zr–Nb–Sn–Fe alloy over the annealed Zr–Nb–O alloy. However, the creep ductility was found to be greater in annealed Zr–Nb–O than in stress-relieved Zr–Nb–Sn–Fe.

(3) Zr–Nb–O alloy was found to have stress exponents of 5–7 independent of stress level in the steady-state creep region whereas Zr–Nb–Sn–Fe alloy exhibited the transition of the stress exponent from 6.5 to 7.5 in the lower stress range to ~4.2 in the higher stress range. The constancy of stress exponent in Zr–Nb–O alloy tubes strongly supports that the decrease of the stress exponent with increasing stress in Zr–Nb–Sn–Fe is associated with the presence of Sn atoms.

(4) The activation energies for creep deformation were calculated to be between 240 and 260 kJ/mol for the Zr–Nb–Sn–Fe alloy, while those were between 240 and 280 kJ/mol for the Zr–Nb–O alloy. The slightly greater creep activation energy in Zr–Nb–O is thought to be attributed to the lower contribution of grain boundary diffusion due to a lager grain size.

(5) The difference of LMP between annealed Zr–Nb–O and stress-relieved Zr–Nb–Sn–Fe is not large considering the large difference of strength level between annealed Zr–Nb–O and annealed stress-relieved Zr–Nb–Sn–Fe. The better-than-expected creep life of annealed Zr–Nb–O alloy with a lower strength can be attributable to the combined effects of creep ductility enhancement associated with softening and the decreased contribution of grain boundary diffusion due to the increased grain size.

Acknowledgements

This research was supported by Basic Atomic Energy Research Institute Program through the National Research Foundation of Korea (NRF) funded by the Ministry of Education, Science and Technology (2009-0075917).

References

[1] J.A.L. Robertson, J. Nucl. Mater. 100 (1981) 108.
[2] E. Tenckhoff, P.L. Rittenhouse, J. Nucl. Mater. 35 (1970) 14.
[3] E.F. Ibrahim, R. Choubey, J.J. Jonas, J. Nucl. Mater. 126 (1984) 44.
[4] R.A. Holt, J. Nucl. Mater. 159 (1988) 310.
[5] W. Liu, Q. Li, B. Zhou, Q. Yan, M. Yao, J. Nucl. Mater. 341 (2005) 97.
[6] K.N. Choo, Y.H. Kang, S.I. Pyun, V.F. Urbanic, J. Nucl. Mater. 326 (2004) 86.
[7] T.S. Byun, K. Farrell, J. Nucl. Mater. 209 (1994) 226.
[8] R.A. Holt, J. Nucl. Mater. 51 (1974) 309.
[9] R.A. Holt, J. Nucl. Mater. 50 (1974) 207.
[10] K.W. Lee, S.K. Kim, K.T. Kim, S.I. Hong, J. Nucl. Mater. 295 (2001) 21.
[11] S.Y. Lee, K.T. Kim, S.I. Hong, J. Nucl. Mater. 392 (2009) 63.
[12] S.I. Hong, K.W. Lee, J. Nucl. Mater. 340 (2005) 203.
[13] G.P. Sabol, G.R. Kilp, M.G. Balfour, E. Roberts, ASTM STP 1023 (1989) 227.
[14] D.O. Northwood, X. Meng, B.O. Warr, ASTM STP 1132 (1991) 156.
[15] J. Weertman, AIME 218 (1960) 207.
[16] D. Kaddour, S. Frechinet, A.F. Gourgues, J.C. Brachet, L. Portier, A. Pineau, J. Nucl. Mater. 51 (2004) 515.
[17] J.D. Lubahn, R.P. Felgar, Plast. Creep Metal. (1961) 210.
[18] F.A. Mohamed, T.G. Langdon, Acta Metall. 22 (1974) 779.
[19] P. Yavari, F.A. Mohamed, T.G. Langdon, Acta Metall. 29 (1981) 1495.
[20] S.I. Hong, Mater. Sci. Eng. 86 (1987) 211.
[21] S.I. Hong, Mater. Sci. Eng. 91 (1987) 137.
[22] S.I. Hong, Mater. Sci. Eng. 82 (1986) 175.
[23] S.I. Hong, Mater. Sci. Eng. 79 (1986) 1.
[24] O.S. Ivanov, U.K. Grigorovitch, in: Second International Conference on Peaceful Uses of Atomic Energy, Genova, vol. 5, 1958, p. 34.
[25] W.A. Mcinteer, David L. Baty, K.O. Stein, ASTM STP 1023 (1989) 621.
[26] S.I. Hong, C. Laird, Acta Metall. Mater. 38 (1990) 1581.
[27] S.I. Hong, W.S. Ryu, C.S. Rim, J. Nucl. Mater. 120 (1984) 1.
[28] S.I. Hong, W.S. Ryu, C.S. Rim, J. Nucl. Mater. 116 (1983) 314.
[29] J.J. Holmes, J. Nucl. Mater. 13 (1964) 137.
[30] M. Pahutova, J. Cadek, Mater. Sci. Eng. 11 (1973) 151.
[31] S.W. Nam, S.I. Hong, D.H. Shin, J. Mater. Sci. 18 (1983) 1743.
[32] M.C. Naik, R.P. Agarwala, Acta Metall. 15 (1967) 1521.
[33] G.M. Hood, R.J. Schultz, Acta Metall. 22 (1974) 459.
[34] F.R. Larson, J. Miller, Trans. ASME 74 (1952) 74.
[35] M. Mayuzumi, T. Onchi, J. Nucl. Mater. 175 (1990) 135.